Available online at www.sciencedirect.com

ScienceDirect

Advances in Space Research 73 (2024) 4922–4936

ADVANCES IN SPACE RESEARCH (a COSPAR publication)

www.elsevier.com/locate/asr

Spatiotemporal variability of the coastal circulation in the northern Gulf of Cadiz from Copernicus Sentinel-3A satellite radar altimetry measurements

R. Mulero-Martinez [a,*], J. Gómez-Enri [a], L. De Oliveira Júnior [b], E. Garel [b], P. Relvas [c], R. Mañanes [a]

[a] Department of Applied Physics, Faculty of Marine and Environmental Sciences, University of Cadiz, Puerto Real, 11510, Spain
[b] Centre for Marine and Environmental Research (CIMA), University of Algarve, Faro 8005-139, Portugal
[c] Centre of Marine Sciences (CCMAR), University of Algarve, Faro 8005-139, Portugal

Received 29 November 2023; received in revised form 24 February 2024; accepted 27 February 2024
Available online 8 March 2024

Abstract

This study presents a generalised characterisation of the surface circulation over the northern shelf of the Gulf of Cadiz, based on 4 years of high-resolution satellite altimetry data from Sentinel-3A and wind model data. The altimetry-based surface zonal currents, adjusted for bottom-drag and wind effects, are compared with a generic CMEMS product and validated against in-situ ADCP measurements. The proposed altimetry product demonstrates superior performance than the CMEMS product, accurately reflecting surface circulation direction compared to in-situ measurements ($r = 0.77$, RMSE = 0.10 m/s, bias = 0.01 m/s). The use of the bottom-drag and wind-corrected/uncorrected altimetry product for spatiotemporal analysis of the shelf circulation revealed the distinct contributions of wind-driven and geostrophic components in different basin sectors. The results show that over the western basin, positive (eastward) surface currents were predominantly driven by westerly winds, while only occasionally, westward flows coincided with easterly winds, suggesting a higher control of the geostrophic component over the westward flows. In contrast, over the eastern basin, both eastward and westward flows were found to be primarily driven by favourable winds. Additionally, the analysis of Absolute Dynamic Topography (ADT) values along the whole basin showed the presence of ADT gradients both along-shore and cross-shore over the shelf, contributing to geostrophic flows. Finally, the seasonal analysis showed that eastward circulation tends to dominate during the spring and summer months, related to the upwelling season in the Gulf of Cadiz and associated westerly winds. Westward flows prevail during the winter months, related to easterly winds and the rebalancing of the along-shore sea level gradient during relaxed upwelling conditions. The findings demonstrate a significant improvement in the use of satellite altimetry data to study complex oceanographic dynamics in coastal areas, where both spatial and temporal variability are high. Moreover, the similarity of our results to those obtained from in-situ systems supports the use of altimetry data and publicly available wind models to support oceanographic studies in remote or resource-limited areas.

Keywords: Coastal altimetry; Coastal oceanography; Sentinel-3; Gulf of Cadiz; Surface circulation; Wind speed

1. Introduction

The use of satellite altimetry had a transformative impact on the discipline of physical oceanography by providing a comprehensive global perspective on ocean

* Corresponding author.
E-mail addresses: roberto.mulero@uca.es (R. Mulero-Martinez), jesus.gomez@uca.es (J. Gómez-Enri), lojunior@ualg.pt (L. De Oliveira Júnior), egarel@ualg.pt (E. Garel), prelvas@ualg.pt (P. Relvas), rafael.salinas@uca.es (R. Mañanes).

https://doi.org/10.1016/j.asr.2024.02.054
0273-1177/

topography from space (Fu et al., 2010). This advancement has made significant contributions to our understanding of large-scale circulation patterns and processes in the open ocean through the application of geostrophic approximation methods. Studying ocean dynamics becomes notably complex in coastal areas and smaller sub-basins where the geostrophic approximation by itself might not be enough to explain the circulation due to local phenomena and non-geostrophic factors like complex variations in wind fields, shallow bottom topographies, river discharges, and interactions between different water masses (Criado-Aldeanueva et al., 2006; Mulero-Martínez et al., 2021). Nonetheless, more in-depth knowledge of the ocean dynamics over coastal areas (including the potential effects of sea level rise) has significant socio-economic and environmental implications, potentially improving the management of activities such as fisheries, offshore energy or navigation-related risks.

Recent advancements in radar altimetry have greatly enhanced the accuracy and resolution of sea surface height (SSH) measurements along the satellite's tracks, allowing the study of coastal ocean circulation by providing observations at short spatial scales critical for coastal regions (Morrow et al., 2017; Raney, 2012). In particular, Synthetic Aperture Radar (SAR) Delay-Doppler altimetry achieves a resolution which is an order of magnitude finer compared to conventional radar altimetry. The Sentinel-3A (S3A) satellite altimeter currently provides SAR-mode data in the whole ocean enabling the application of this innovative data processing approach to coastal ocean studies (Feng et al., 2023). Besides, satellite altimetry continues evolving and represents a fast-developing technology, exemplified by the recent launch of the Surface Water and Ocean Topography (SWOT) mission that will collect data across a 120 km wide swath (Srinivasan and Tsontos, 2023).

This study aims to present the capacities of S3A SAR mode datasets for assessing coastal sea surface circulation over the Gulf of Cadiz. In addition, the study shows how the value of such a dataset, characterised by its enhanced and consistent time and spatial coverage, can be improved when accounting for the effect of ageostrophic factors such as the bottom-drag effects and the wind-driven surface circulation. On a final basis, this work aims to contribute to achieving a level of understanding of ocean circulation in coastal zones from altimetry similar to that of the open ocean (Troupin et al., 2015), even in areas with a lack of either in-situ measurements or local hydrodynamical models. The overarching goal of this study is to complement regional coastal oceanographic studies by providing the highest quality altimeter measurements of Absolute Dynamic Topography (ADT) and ADT-derived geostrophic current (V_t), over the northern GoC coastal zone. This objective entails an investigation into the quality of different altimetry-based products but also about the different mechanisms affecting the sea surface circulation over the continental shelf of the GoC along its sub-basins. The approach relies upon previous coastal oceanographic studies (Manso-Narvarte et al., 2018; Mulero-Martínez et al., 2021) based on altimetry and local oceanographic studies (Garel et al., 2016; De Oliveira Júnior et al., 2021; De Oliveira Júnior et al., 2022) based on various measurement devices such as high-frequency radar (HFR) and Acoustic Doppler current profiler (ADCP).

The paper is organized as follows. Section 2 provides a concise overview of the study region and presents recent research findings about the ocean circulation in the area. Section 3 describes the datasets and methods applied, including the detailed filtering strategy applied to the raw altimetry data and the approach to obtain estimates of the geostrophic velocity. Results and discussions are presented in Section 4, starting with the comparison of altimetry-derived surface current velocity from different products with in-situ ADCP measurements. Next, the GoC shelf circulation is characterised based on current velocity estimated with the most accurate product from the previous comparison with ADCP, including the assessment of the alongshore ADT gradients, the different contributions of both the bottom-drag corrected geostrophic and the wind-driven circulation to the total circulation and the spatiotemporal variability of the circulation over the shelf. Finally, the summary and conclusions are presented in Section 5.

2. Study area

The GoC is located between the northwestern coast of Africa and the southwestern tip of the Iberian Peninsula. The northern shelf spans from the eastern Strait of Gibraltar to Cape San Vicente (CSV) in the west. It is divided by Cape Santa Maria (CSM) into a narrower western shelf and a broader eastern shelf (Fig. 1). The complex dynamics of the surface circulation in this region are influenced by factors such as bathymetry, wind patterns, river discharges and water mass exchanges through the Strait of Gibraltar (Criado-Aldeanueva et al., 2006; García-Lafuente et al., 2006).

The wind field along the GoC is influenced by various factors, including topography, atmospheric flows, and temperature variations between land and sea (Carvalho et al., 2014; Mulero-martinez et al., 2022a, 2022b). The wind patterns in the GoC exhibit alternating flows known as Ponientes (westerly) and Levantes (easterly). These winds can occur consistently throughout the year with a periodicity of approximately 2–3 days (De Oliveira Júnior et al., 2021) but generally respond to a seasonal cycle forced by the seasonal displacement of the Azores high (Criado-Aldeanueva et al., 2009; Ortega et al., 2023). During the winter and autumn months (December to February and September to November, respectively), there is a high degree of variability in wind direction accompanied by frequent intense weather events, including strong Levantes. In spring, northwest winds become less dominant, occasionally giving way to stronger eastward winds. Summer experiences predominantly calm winds with a prevailing

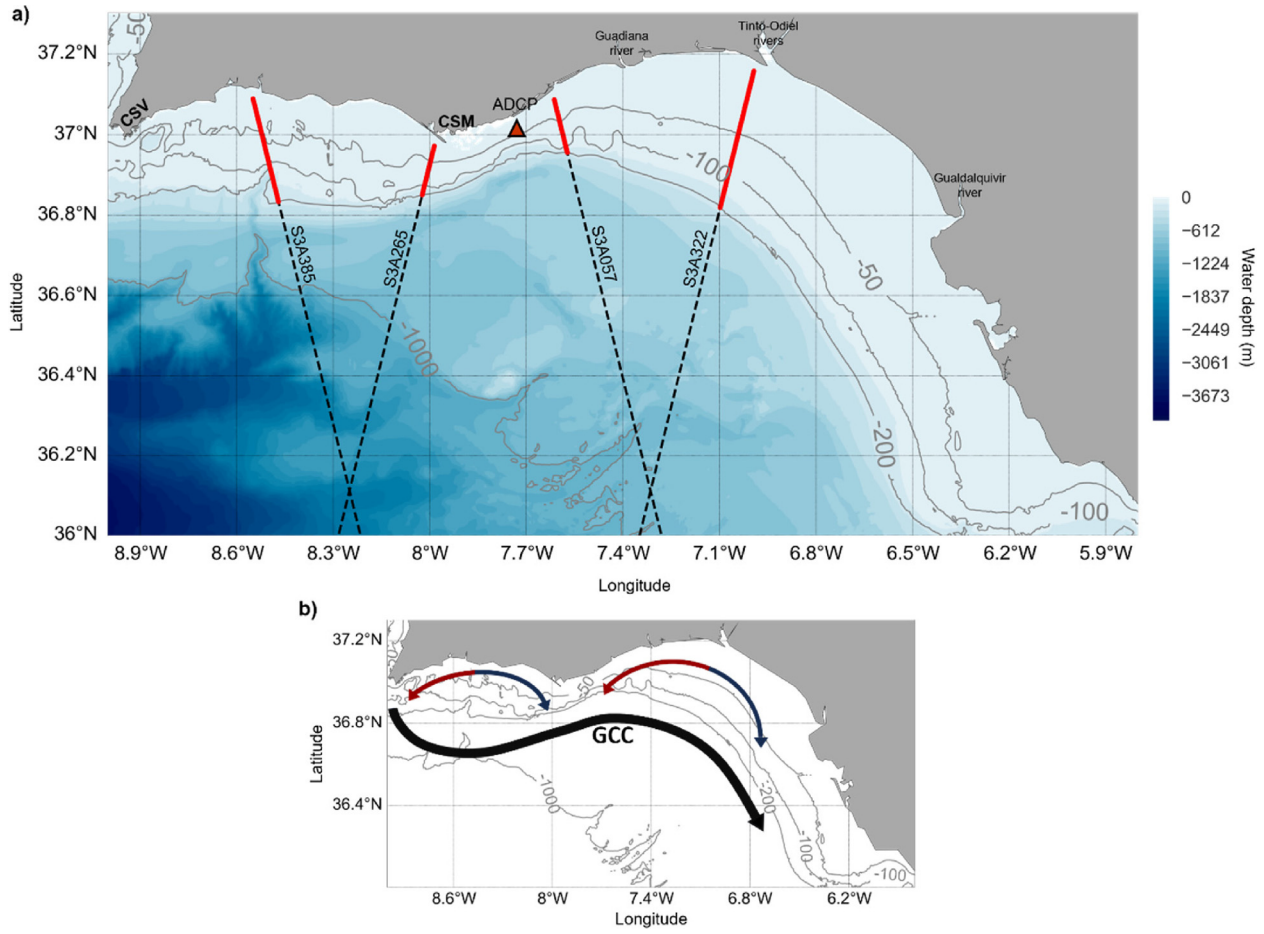

Fig. 1. (a) Study area along with the Sentinel-3A tracks (red lines indicate the sectors considered over the continental shelf, with depth $\leq$ 200 m) selected for the study and the location of the Armona ADCP. The main geographical characters are also presented: Cape San Vicente (CSV); Cape Santa Maria (CSM). (b) Representative scheme of the surface circulation in the northern margin of the GoC based on (De Oliveira Júnior et al., 2022), where the GCC remains stable almost all year round, while over the shelf, the blue lines represent the circulation under favourable upwelling conditions and the red lines represent the circulation under weakened upwelling conditions and/or strong Levantes.

northwest component (De Oliveira Júnior et al., 2021). Northerly winds along western Portugal rotate anticlockwise from CSV, providing the conditions for local upwelling along the southern coast. East of Cape Santa Maria, the intensity of the wind-related upwelling events decreases due to the widening continental shelf being non-significant by the middle of the eastern basin (De Oliveira Júnior et al., 2022).

The large-scale (>100 km) sea surface circulation in the GoC generally displays a south-eastward background circulation superimposed on the anticyclonic pattern delineated by the presence of the Gulf of Cadiz Current (GCC) that is strongest in summer (Criado-Aldeanueva et al., 2006; García-Lafuente et al., 2006; Garel et al., 2016; Sánchez and Relvas, 2003). Shifts to northwestward flow can be observed throughout the year, but predominantly in late autumn and early winter, particularly in December and January (Folkard et al., 1997; Sánchez and Relvas, 2003). Over the continental shelf, the flow is alongshore, alternating between eastward and westward at a time scale of 2–3 days, following a similar pattern to the wind field. The alongshore velocities, mostly zonal due to the coastline orientation, can reach up to approximately 0.4 m/s, while cross-shore (meridional) velocities, mainly dominated by tidal forces, are one order of magnitude weaker (Garel et al., 2016; De Oliveira Júnior et al., 2021). The shelf circulation along the GoC is highly linked to the southward flows along Portugal's western coast and its upwelling system. Eastward cold-water flows along the GoC shelf originated either under northerly winds, due to the rotation of the poleward Portugal's current around CSV or locally under westerly wind conditions (Folkard et al., 1997; De Oliveira Júnior et al., 2022). In contrast, westward coastal flows, commonly expressed as Coastal Counter Currents (CCC) (Garel et al., 2016; Laiz et al., 2019; De Oliveira Júnior et al., 2021, 2022; Teles-Machado et al., 2007) due to their opposite direction to the characteristic south-eastward slope of the GCC, develop along a relatively narrow strip spanning up to 15–20 km off the coast (De Oliveira Júnior et al., 2021). Recent studies of surface currents derived from High-Frequency Radar (HFR) and numerical model simulations

found the coastal margin of the westernmost side of the Strait of Gibraltar as the initiation point of the CCCs events (Sirviente et al., 2023). Opposite to the eastward flows, CCCs tend to increase coastal temperatures during summer through the transport of warm water from areas surrounding the mouth of the Guadalquivir River and Cadiz Bay marshes (Relvas and Barton, 2002). Such transport does not only affect water temperature but also nutrient availability and the transport of pollutants throughout the basin, playing a key role in the biogeochemistry of the area (Laiz et al., 2019). The occurrence of CCCs has been associated with an unbalanced along-shore pressure gradient during periods of weakened upwelling-favourable winds (Garel et al., 2016; De Oliveira Júnior et al., 2021, 2022). In addition to local wind stress, it is crucial to take into account the impact of remote factors such as wind forcing over the Alboran Sea and the eastern side of the Strait of Gibraltar. A recent study also suggested a potential relation with the sea level atmospheric pressure forcing over the Ligurian Sea (Sirviente et al., 2023). However, understanding the primary driving mechanisms for CCCs in this region is challenging since those events result from various intricated factors that vary spatially and temporally.

Considering the different features that characterise the GoC circulation, a generic glimpse of the ocean surface circulation can be defined as a predominant anticyclonic system, regarding the open ocean circulation, with episodic inversions to north-westward circulation under strong and persistent easterly winds. The shelf circulation is characterised by the presence of two transient cyclonic cells over the eastern and western basins, driven by CCC events in the north and delimited by the GCC in the south (Criado-Aldeanueva et al., 2009).

3. Data and methods

3.1. Satellite altimetry data from Sentinel-3A

This study is based on high-resolution along-track ADT obtained from Sea Level Anomaly (SLA) measurements from 4 different Sentinel-3A tracks crossing the continental shelf of the GoC (Fig. 1), during the period: 2017–2021. Each track has a repeat cycle of 27 days and is identified by its specific relative orbit number: S3A-385, S3A-265, S3A-057 and S3A-322.

The synthetic aperture radar altimeter (SRAL) instrument onboard Sentinel-3A can measure in two different modes, namely, low resolution (LRM) and synthetic aperture radar (SAR). The latter mode, SAR, is renowned for its high-resolution along-track capabilities and is widely utilised across the global ocean. Additionally, the data from the SRAL instrument on Sentinel-3A can be post-processed to generate level-2 data at frequencies of 1 Hz, 20 Hz and 80 Hz for the Ku and C bands. Detailed information regarding these data can be found in the Sentinel-3 Altimetry Document Library, accessible at https://sentinel.esa.int/web/sentinel. Sentinel-3A level 2 data for this study were accessed through the ESA Earth Console Parallel Processing Service (P-PRO) SAR versatile altimetric toolkit for ocean research and exploitation, known as P-PRO SARvatore (https://ui-ppro.earthconsole.eu). These data were processed using the predefined setup designed for coastal zones. In addition, the retracking process was based on the SAR Altimetry MOde Studies and Applications (SAMOSA++) model (Dinardo et al., 2021). The product extracted consists of SLA measurements at a frequency of 20 Hz, yielding an along-track spatial resolution of approximately 330 m. Finally, a set of range and geophysical corrections, presented in Table 1, are applied following the recommendations in (Feng et al., 2023; Fenoglio-Marc et al., 2015; Gómez-Enri et al., 2018; Mulero-Martínez et al., 2021), including a sea state bias (SSB) correction based on 5 % of the significant wave height (SWH), as suggested by (Fenoglio-Marc et al., 2015; Gómez-Enri et al., 2018).

3.1.1. Sea level anomaly (SLA) filtering strategy

To obtain valid SLA data up to 3 km from the coast over the GoC, 20-Hz along-track SLA data from 4 different Sentinel-3A relative orbits over the area for the period 2017–2021 were edited as follows: Firstly, raw SLA values closer than 3 km to the coastline were rejected to maintain a distance of good quality. This criterion is based on Aldarias et al. (2020), which suggested that good quality data can be obtained within S3-A tracks up to 3 km from the coast in our study area. Secondly, values larger than three times the standard deviation of the SLA were removed and replaced by linearly interpolated values; this process was applied 10 times to remove most outliers in SLA estimates (Bouffard et al., 2010; Meloni et al., 2019; Mulero-Martínez et al., 2021). Finally, a LOESS (locally weighted smoothing) filter (Cleveland and Devlin, 1988) was applied along each track segment individually to filter out high-frequency noise (Manso-Narvarte et al. 2018b); this is a common and proven valid processing procedure for the study of oceanic mesoscale phenomena (Morrow et al., 2017; Mulero-Martínez et al., 2021). After applying this procedure, the resulting SLA is suitable for being used for oceanographic purposes. Fig. 2 shows an example of track S3A-057 before (Fig. 2a) and after (Fig. 2b) the filtering process.

3.1.2. Absolute dynamic topography (ADT) and surface circulation

Absolute dynamic topography (ADT) profiles were estimated by adding the mean dynamic topography (MDT) to the SLA. Though the ADT can also be computed by extracting a geoid model from the sea surface height (SSH), the MDT-based approach has been found to provide the best estimates when used to calculate derived geostrophic velocities, as it is exposed in Section 4.1.1. The DTU15MDT model (Knudsen,Andersen,and Maximenko, 2016) was used to calculate the final ADT. This MDT model has been previously used by (Mulero-Martínez et al., 2021)

Table 1
Range and geophysical corrections applied to the original Sea Level Anomaly (SLA) measurements.

Range corrections	**Geophysical corrections**	
Atmospheric	**Tidal**	**Ocean surface**
Dry Tropospheric	Ocean Tide (TPXO8-atlas model)	Dynamic Atmospheric Correction
Wet Tropospheric	Long-Period Equilibrium Tide	Sea State Bias (5 % Significant Wave Height)
Ionospheric	Ocean Loading Tide	
	Solid Earth Tide	
	Geocentric Polar Tide	

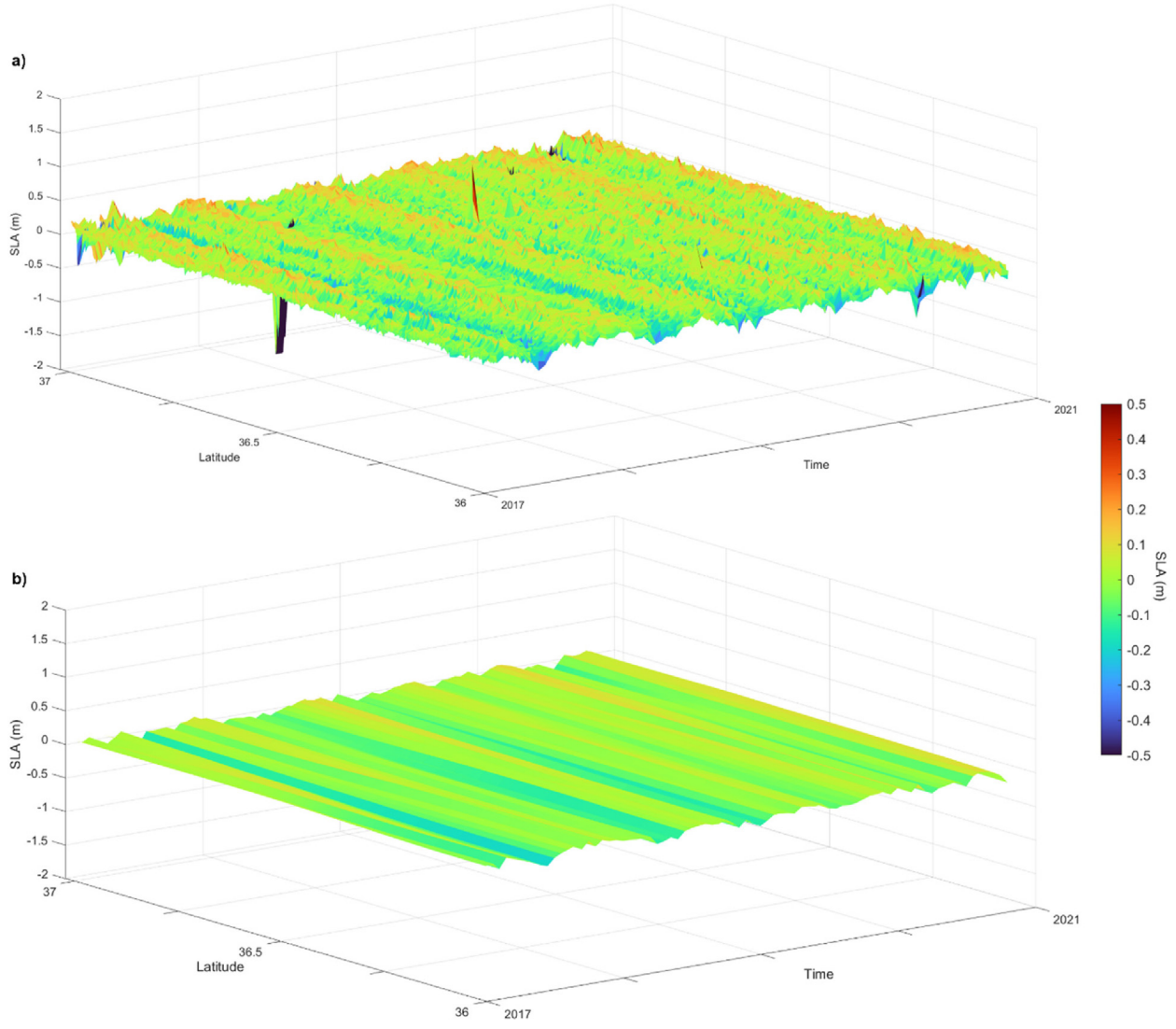

Fig. 2. Latitude-time variability of the SLA from S3A-057 before (a) and after (b) applying the filtering strategy.

over the eastern basin of the GoC for estimating geostrophic currents from CryoSat-2 satellite altimetry data with good results. While the MDT data were interpolated from the original model grid to the satellite' tracks positions, the EGM2008 (Pavlis et al., 2008) and EIGEN6C4 (Förste et al., 2014) geoid models data tested in Section 4.1.1 were extracted along with the raw altimetry data from the P-PRO SARvatore service, at the same 20 Hz posting rate.

Given that the ADT characterises the dynamic signal denoting displacement relative to the equipotential surface (geoid) influenced by interactions involving the atmosphere and the topographical features of the ocean floor and its boundaries, it is feasible to derive an estimate of the absolute surface geostrophic circulation using altimeter measurements. This estimation relies on analysing the spatial fluctuations in ADT while accounting for the impact of

the Earth's rotational motion, represented by the Coriolis force. Briefly, it is possible to obtain estimates of the absolute geostrophic component of the surface circulation (V_{gAbs}) normal to the satellite tracks using the following Eq. (1):

$$V_{gAbs} = \frac{-g}{f} \cdot \frac{\partial ADT}{\partial y} \quad (1)$$

where g ($m \cdot s^{-2}$) is the gravitational acceleration; y (m) is the along-track distance; f (s^{-1}) is the Coriolis parameter ($f = 2\Omega sin\varphi$, where Ω is the angular rotation velocity of the Earth and φ the latitude). The along-track ADT (m) gradient (slope) is estimated by using the optimal filter developed by (Powell and Leben, 2004). In addition, (Mulero-Martínez et al., 2021) suggested that, in coastal areas, the effect of both the wind-induced velocity component and the bottom friction must be considered to improve estimates of the surface circulation. Following (Mulero-Martínez et al., 2021), Eq. (2) and Eq. (3) provide an estimation of the bottom-drag corrected surface geostrophic velocity (V_{gd}, $m \cdot s^{-1}$) and the zonal surface wind-driven velocities (V_w, $m \cdot s^{-1}$), respectively:

$$V_{gd} = \frac{-g}{\left(f + \frac{r^2}{f}\right)} \cdot \frac{\partial ADT}{\partial y} \quad (2)$$

$$V_w = 0.03 \cdot U_{10} \cdot \cos\left(10^{\circ}\right) \quad (3)$$

where $r = (0.35C_d)/d$ (m^{-1}) is a depth-dependent parameter, using a typically accepted value of $C_d = 2.0\ 10^{-3}$ (Bowden, 1983), and U_{10} ($m \cdot s^{-1}$) is the zonal component of the wind speed at 10 m above the mean sea level.

Finally, Eq. (4) allows the estimation of a more complete along-track total surface velocity (V_t), accounting for the main geostrophic component derived from altimetry and corrected for the bottom friction and wind drag effects on the surface circulation, as proposed by (Mulero-Martínez et al., 2021).

$$V_t = \frac{-g}{\left(f + \frac{r^2}{f}\right)} \cdot \frac{\partial ADT}{\partial y} + 0.03 \cdot U_{10} \cdot \cos\left(10^{\circ}\right) \quad (4)$$

where r is a depth-dependent parameter and U_{10} is the zonal component of the wind speed. An in-depth development of Eq. (2) can be found in (Mulero-Martínez et al., 2021). In addition, the resulting cross-track velocities are rotated to obtain the zonal component of the current.

Fig. 3 summarizes the complete methodology from the original raw SLA measurements to the final V_t product.

3.2. Model wind data

Wind data used to compute the wind component of the circulation for the period 2017–2021 was extracted from the National Center for Environmental Prediction (NCEP) operational Global Forecast System (GFS) with 0.25° (approximately 25 km) of grid resolution and 6 h of temporal sampling (https://rda.ucar.edu/datasets/ds084.1/). A previous study on the GoC found the NCEP-GFS model as a reliable source of wind data, obtaining the best results in terms of error and correlation, for both wind speed and direction, when assessed against in-situ measurements and compared with other equivalent publicly available models (Carvalho et al., 2014). NCEP GFS wind data was used for the estimation of the wind-driven surface current in Section 4.2. However, for the detailed evaluation of surface current velocities from different altimetry-based products against ADCP measurements during the period 2020–2021, presented in Section 4.1, an alternative source with higher spatial and temporal resolutions, and locally calibrated, was used to accurately reproduce the wind conditions, though with a higher computation cost. Specifically, the wind data for the study was obtained using the Weather Research and Forecasting (WRF) model v.4.2 (Skamarock and Klemp, 2019), which is a mesoscale non-hydrostatic model. The WRF model was used to produce dynamically downscaled hourly 10 m wind speed and direction over the complete GoC area. The 3 km resolution domain was one-way nested within a larger parent domain with a resolution of 9 km. The initial and boundary conditions were provided by the NCEP-GFS model described earlier and applied to the parent domain. The dynamical set-up of the simulations follows the scheme presented in (Mulero-martinez et al., 2022a,2022b), as it was proved to successfully reproduce the wind conditions in the area.

3.3. In-situ ADCP measurements

Acoustic Doppler current profiler (ADCP) measurements were obtained from Armona coastal station (37.0108°N, 7.7413°W) (Fig. 1), where the water depth is 22 m. For the data collection a Sentinel V 500 kHz ADCP, manufactured by TRDI, was bottom-mounted 4 times for periods ranging from January 2020 to December 2021. The instrument recorded hourly velocities in cells of 0.5 m thick along the water column. The resulting data was de-tided by applying a low-pass filter of a 40-h cut-off period. This study was based only on the spatial average of the two uppermost valid cells (Garel et al., 2016), typically within the initial 2 to 3 m from the water surface. For the comparisons against satellite altimetry data, presented in Section 4.1, 72 h averages of ADCP measurements previous to the satellite pass were used. Using 72 h averages is suggested in (Mulero-Martínez et al., 2021; Roesler, Emery, and Kim, 2013) for comparisons with altimetry data since it is representative of a synoptic circulation, similar to the estimates using altimetry data, mainly based on geostrophic processes.

3.4. CMEMS gridded product

Gridded absolute geostrophic current velocities were gathered from the Copernicus Marine Environment Monitoring Service (CMEMS). The gridded product is based on multi-mission satellite altimetry (including Sentinel-3A) SLA measurements. The final gridded data is esti-

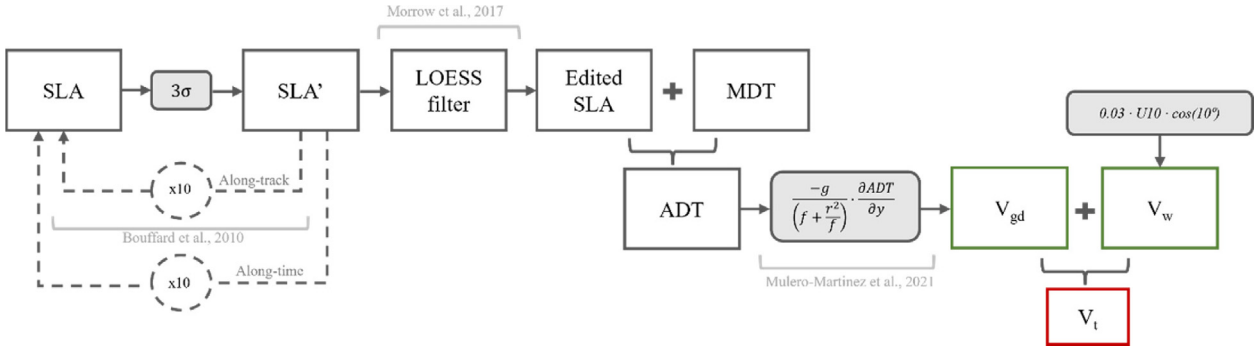

Fig. 3. Schematic representation of the complete methodology for editing satellite sea level anomaly and calculating the along-track total surface velocity.

mated by optimal interpolation, merging the level-3 along-track measurement from the different altimeter missions available and providing daily estimates with a 1/8°x1/8° spatial resolution. A more detailed description of the development and quality of the products can be found in https://doi.org/10.48670/moi-00142.

4. Results and discussion

4.1. Comparison and validation with in-situ current measurements

The S3A-057 satellite track passes over the GoC southbound (descending track), covering a narrow part of the continental shelf east of the CSM (Fig. 1). The Armona ADCP was moored 15 km from this track. Different surface current estimates from S3A-057 altimetry measurements and gridded CMEMS products were compared with in situ measurements from the ADCP moored at Armona station.

4.1.1. Evaluation of ADT constructions

Results of the comparison between ADCP surface zonal velocities and the three different S3-V_t products, computed with ADTs from the different approaches (S3-V_tMDT, S3-V_tEGM and S3-V_tEIGEN), are presented in Fig. 4. The comparison of different methods yielded the best result in terms of Pearson's correlation and root mean square error when using S3-V_tMDT (correlation coefficient = 0.77; RMSE = 0.10 m/s). The S3-V_tEGM and S3-V_tEIGEN estimates also performed well but had slightly lower correlation coefficients and larger RMSE compared to S3-V_tMDT. This finding aligns with a previous study (Feng et al., 2023) conducted in the Northwest Atlantic Shelf, particularly in the Gulf of Maine, which also concluded that constructing ADT based on MDT provides more accurate results when used for geostrophic current estimations, mainly due to increasing geoid errors near the coast.

4.1.2. Inter-products comparison

The comparison presented in Fig. 5 shows the current velocity estimated from several altimetry-based products against in-situ ADCP surface current measurements. Specifically, the altimetry-based products are the bottom-friction corrected geostrophic current (V_{gd}), the total current velocity accounting for the bottom-friction corrected geostrophic and wind components (V_t), generated from both high-resolution altimetry data along S3A-057 (S3-V_{gd} and S3-V_t) and the CMEMS product (C-V_{gd} and C-V_t). The wind information used for the estimation of the V_t was extracted from the high-resolution locally downscaled WRF model. The statistical parameters resulting from the comparison (r-correlation, RMSE, and bias) used to quantify the performance of the different products are presented in Table 2.

The comparison with in-situ measurements shows that the C-V_{gd} product produced the worst results (r = 0.10, RMSE = 0.14 m/s, Bias = −0.01 m/s), which is expected considering that it mainly represents the geostrophic current, corrected only for the bottom friction, in addition to the low resolution and high smoothing of both the final product and altimetric data (1 Hz) used for its development. The CMEMS product improved when applying an estimate of surface wind current (C-V_t), (r = 0.62, RMSE = 0.12 m/s, Bias = 0.01 m/s), especially in terms of correlation. This improvement is due to the greater similarity between the compared variables, resulting from the important role of the wind on the surface circulation of the GoC (Mulero-Martínez et al., 2021; De Oliveira Júnior et al., 2022).

The best results of the comparison derive from the use of the products generated with high-resolution altimetric measurements (20 Hz), S3-V_{gd} and S3-V_t. S3-V_{gd} showed a higher correlation than C-V_t, even without the application of wind current estimation (r = 0.67, RMSE = 0.11 m/s, Bias = 0.03 m/s). The higher spatial resolution of the altimetric data used to generate this product allows for a better representation of nearshore circulation along the continental shelf. However, the lack of a wind component penalizes the results of this comparison in terms of bias. Finally, the S3-V_t product provided the best representation of the surface circulation, with the best results for all calculated statistics (r = 0.77, RMSE = 0.10 m/s, Bias = 0.01 m/s). The S3-V_t product not only has the advantage of being generated with high spatial resolution altimetric data but also includes the variability provided by the estimation of

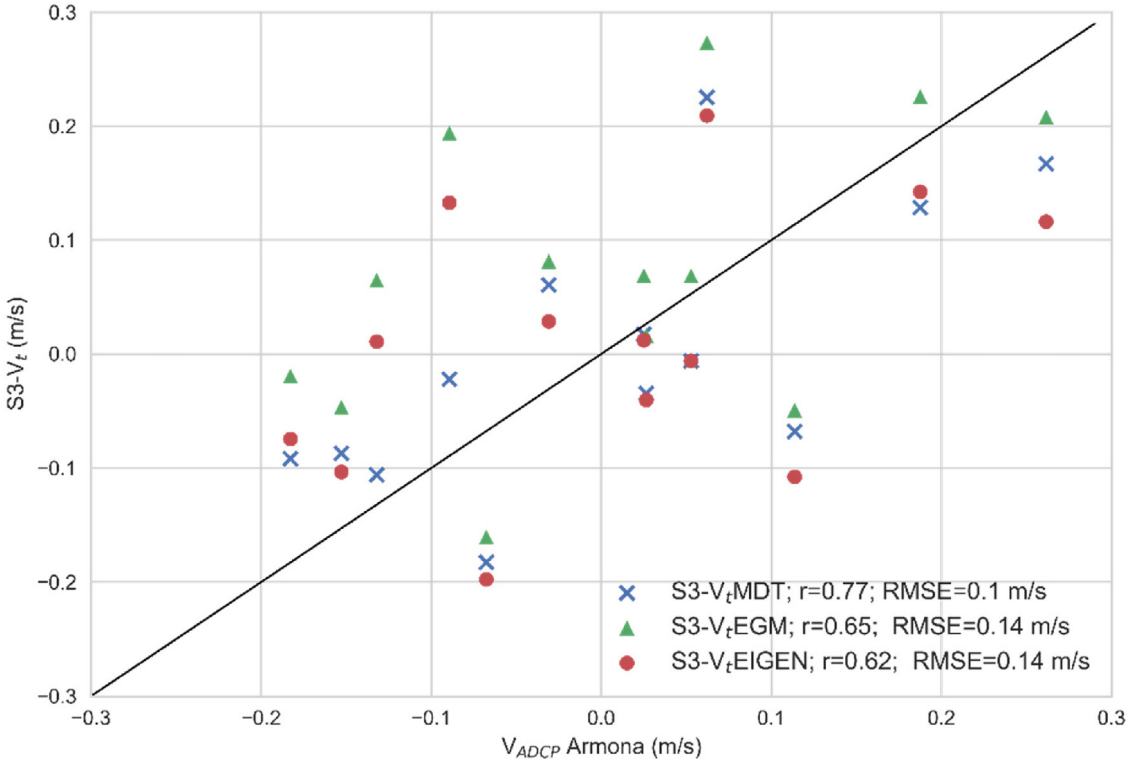

Fig. 4. Scatter plot of the different satellite altimetry-derived surface geostrophic velocity approaches against in-situ ADCP measurements. S3-V$_t$MDT refers to geostrophic velocities estimated using the ADT based on MDT, while S3-V$_t$EGM and S3-V$_t$EIGEN refer to the geostrophic velocities estimated using geoid models EGM2008 and EIGEN6C4, respectively.

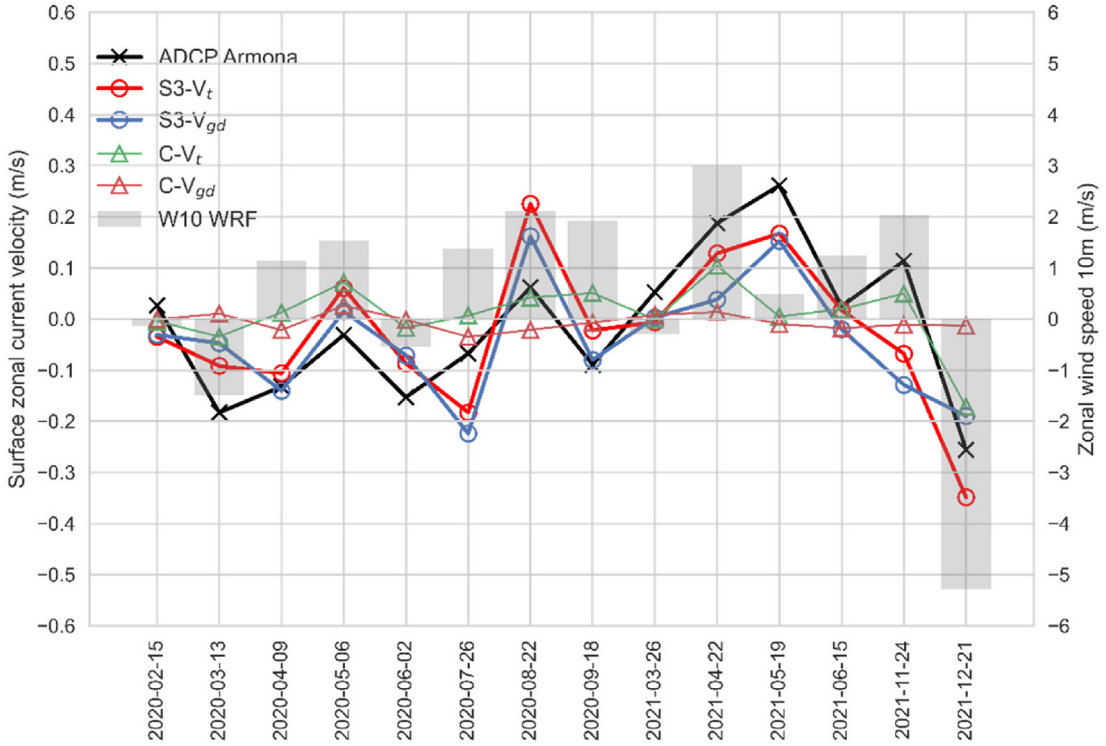

Fig. 5. Match-up time series of altimetry-based current velocities (S3-V$_{gd}$, S3-V$_t$, C-V$_{gd}$, C-V$_t$) and in-situ ADCP Armona surface current velocities, along with the simultaneous zonal wind speed from WRF. Note that the time interval is not constant.

Table 2
Statistical results (correlation coefficient, r; root mean square error, RMSE; and bias, Bias) from the comparison between altimetry-based current velocities (S3-V_{gd}, S3-V_t, C-V_{gd}, C-V_t) and in-situ ADCP Armona surface current velocities.

Product	r	p-value	RMSE (m/s)	Bias (m/s)
C-V_{gd}	0.10	0.742	0.14	−0.01
C-V_t	0.62	0.018	0.12	0.01
S3-V_{gd}	0.67	0.009	0.11	0.03
S3-V_t	0.77	0.001	0.10	0.01

the wind-induced current component. The high variability of the zonal circulation in the continental shelf sector during the analysis period can be observed. This variability, which is highly dependent on the wind field in the area, is well represented by the S3-V_t product, which correctly reproduced the ADCP current direction more than 70 % of the time, even considering weak flows that might be produced by surface gradients of low magnitude, difficult to be resolved by altimetry (Marechal et al., 2020).

Despite the good results, it should be noted that the comparison shows current values obtained independently and in various ways. The ADCP measures at a single point and directly measures the total circulation that is taking place at each moment, while the altimetric products estimate the geostrophic component of the circulation based on the elevation gradient of the ocean surface along the satellite track (Feng et al., 2023). In addition, the distance between the satellite track and the ADCP could also affect the comparison. Such differences stand a limitation when performing this kind of comparison and should be considered when interpreting the statistical results. These results demonstrate the benefits of including the wind effect in the estimation of the surface circulation from altimetry.

4.2. Characterisation of the GoC shelf circulation

Since S3-V_t showed the best validation results, the same methodology has been extended to tracks S3A-385, 265, and 322, in addition to the already mentioned 057, for a longer period: 2017–2021. The use of different satellite tracks along the area allows for analysing the spatiotemporal variability of the surface circulation along the continental shelf in the GoC. It is worth mentioning that unlike in the previous section, the S3-V_t products analysed in this section, have been generated with an estimation of the wind-induced surface current (V_w) based on lower resolution data from NCEP-GFS instead of the locally calibrated WRF downscaling, due to computation limitations. Since the NCEP-GFS was used as boundary conditions for the WRF model, they were found to equivalently represent the synoptic conditions.

4.2.1. Contribution of the geostrophic and wind components

The different timeseries presented in Fig. 6 show the along-track average zonal circulation along the continental shelf of the GoC, from tracks S3A-385 (a), 265 (b), 057 (c) and 322 (d), respectively. Specifically, estimates of the total current (V_t), the bottom-friction corrected geostrophic components (V_{gd}) and the wind component (V_w) of the surface circulation are presented to provide a comprehensive understanding of how the different components contribute to the alongshore circulation in the GoC northern shelf.

Tracks S3A-285, 265 and 057 (Fig. 6a–c) present similar characteristics regarding the contribution of V_{gd} and V_w to V_t. Positive flows are mainly driven by westerly winds, as indicated by the correspondence of positive V_t and V_w, agreeing with the wind field over the area, since west of CSM westerly and north-westerly winds dominate (Folkard et al., 1997; De Oliveira Júnior et al., 2022), while easterlies are less recurrent and weaker than over the southern part of the eastern basin (Mulero-martinez et al., 2022a, 2022b). In contrast, westward V_t flows are likely to occur along with both westward V_{gd} and V_w, but also just linked to V_{gd}, suggesting that westward flows, such as CCCs, are not necessarily linked to strong easterly winds, but also to geostrophic adjustments. Marked events (E1, 2, 3, 4 and 5) in Fig. 6a represent the different scenarios detected with track S3A-385 along the western basin regarding the contribution of both V_{gd} and V_w to the westward flows. Events E1 (21-Apr-2017), E4 (25-Feb-2019) and E5 (23-Feb-2021) show V_t negative flow events driven by both westward V_{gd} and V_w, while during events E2 (30-Sep-2017) and E3 (6-Dec-2018) the V_t flows directed to the west are purely controlled by a negative V_{gd} flow. Several authors have suggested the existence of an alongshore pressure (sea level) gradient over the shelf that is likely to promote westward flows without favourable winds and would explain most of the flow variability during CCCs events in the western basin (Garel et al., 2016; De Oliveira Júnior et al., 2021, 2022). The new findings show that the cross-shore gradients may contribute as well to these events. The actual presence of both sea level gradients (i.e., cross-shore and alongshore) over the shelf is further analysed in Section 4.2.2. Regarding track S3A-322 (Fig. 6d), crossing the eastern basin of the GoC, both V_{gd} and V_w components agree on most of the occasions on the direction of the circulation, aligning with V_t. This observation suggests that in contrast to the western basin, both eastward and westward flows along the shelf in this region are predominantly driven by favourable winds as suggested by previous studies using ADCP measurements (Criado-Aldeanueva et al., 2009). These winds also contribute to the development of cross-shelf sea level gradients through the piling up or down of water at the coast by Ekman transport, as previously reported in nearby areas (Gómez-Enri et al., 2019), which enhances the total flow through the additional contribution of a geostrophic component. The different V_{gd}-V_w interplays along the different basins are reassured when comparing with ADCP measurements with the correlation coefficients for V_{gd}-V_w, being 0.12 for S3A-385 (western basin) and 0.46 for S3A-322 (eastern basin). It can be also observed that, on average,

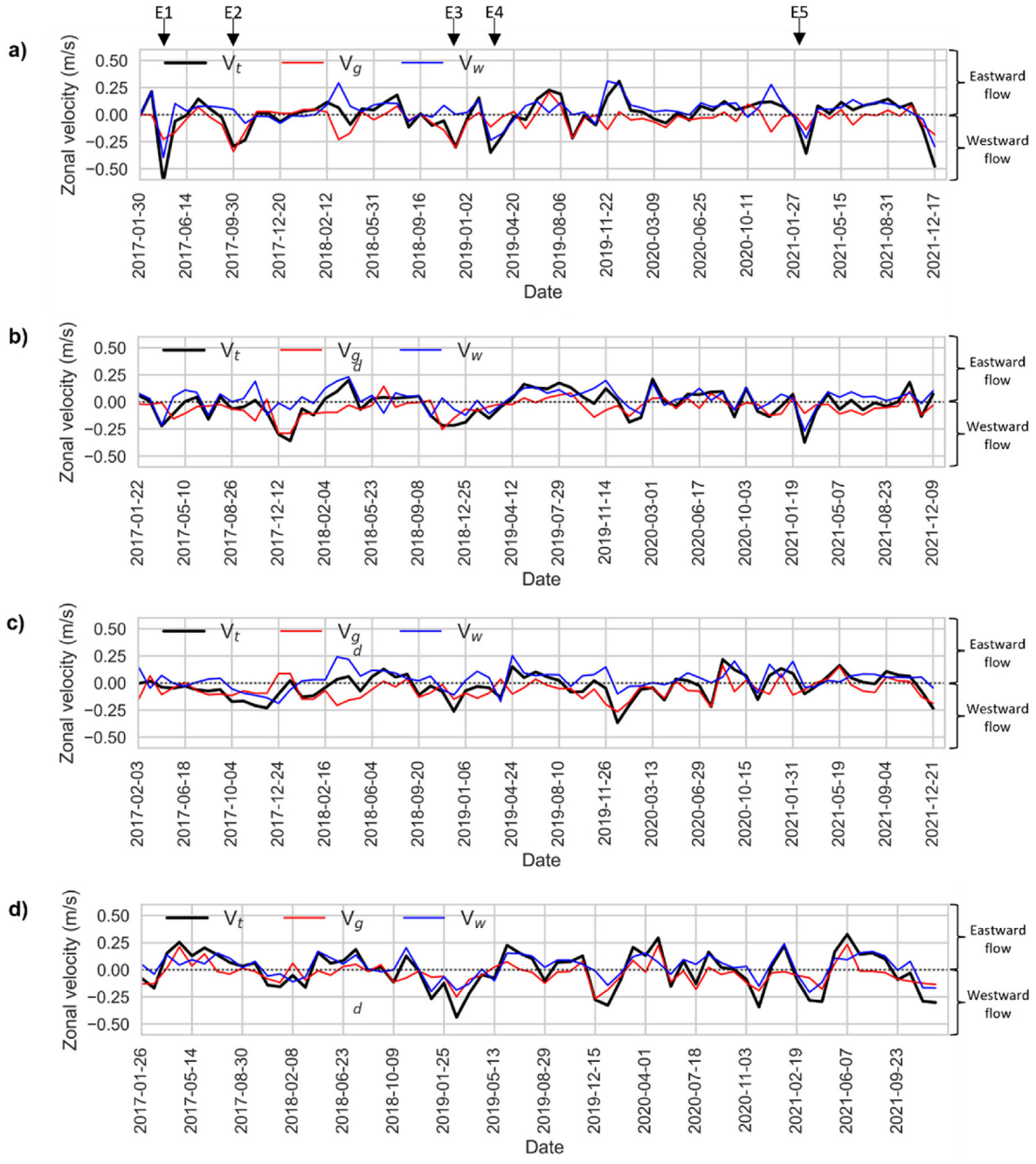

Fig. 6. Time series of shelf average V_{gd} (red lines), V_w (blue lines) and V_t (black lines) from tracks S3A-385 (a), S3A-265 (b), S3A-057 (c) and 322 (d).

the wind-driven flow is eastward for all the tracks, due to the dominance of westerly winds over the area, while the geostrophic flow tends to be westward along the whole basin.

4.2.2. Alongshore and cross-shore sea level gradients

The 5 years average (2017–2021) of ADT for the continental shelf sector traversed by the different tracks is presented in Fig. 7. The results show the existence of ADT gradients both alongshore and cross-shore, the former of much larger amplitude. Alongshore ADT average differences reach up to 4 cm between the easternmost and the westernmost tracks. This result is in line with previous studies, such as (Relvas and Barton, 2002; Sánchez et al., 2006), that estimated an average slope of 5 cm/100 km for the same area based on tide gauges. This difference in ADT along the basin implies the existence of an unbalance in the along-shore pressure gradient. To be rebalanced, such alongshore gradient would lead to a westward flow (García-Lafuente et al., 2006; De Oliveira Júnior et al.,

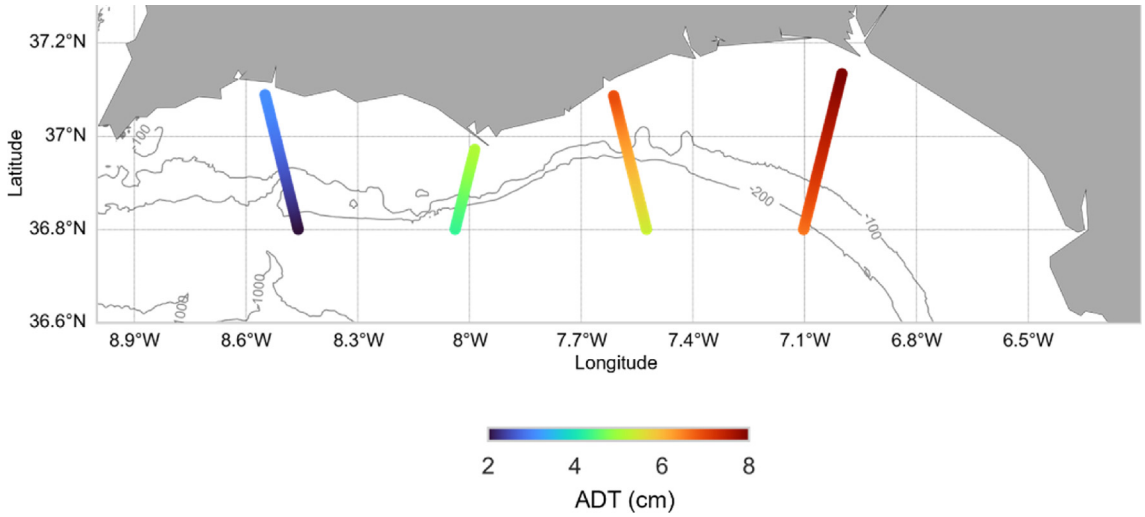

Fig. 7. Along-track ADT average for the period 2017–2021 over the continental shelf of the GoC.

2021) during periods of weakened westerly winds and would be enhanced under easterly wind conditions. Additionally, the cross-shore sea level gradients would also support the westward circulation over the shelf, as for the physical basis of this research, a north–south ADT gradient (higher ADT values close to the coast and lower off the coast) would develop a westward geostrophic flow. Such interpretation of the potential effects of the alongshore and cross-shore sea level gradients (ADT gradients) matches with the previously analysed contribution of the different components to the total shelf circulation at the different locations. The results also agree with several studies that suggested the existence of an alongshore pressure gradient as the main factor driving the commonly known coastal countercurrent (CCC) over the GoC shelf during weak wind conditions (Garel et al., 2016; De Oliveira Júnior et al., 2021,2022) and with the observations from (Sirviente et al., 2023) of sea surface height across-shore gradients directed seawards for days when the CCC in the GoC is present. The average net geostrophic flow resulting from the existence of the ADT gradients presented in Fig. 7 can be summed up as a westward flow in the absence of any other components. Such a flow would support the circulation represented by red lines in Fig. 1.

4.2.3. Spatio-temporal variability

The spatial and temporal variability of the zonal component of surface circulation along the GoC is evaluated by a Hovmöller (HM) diagram (Fig. 8). The figure shows an HM diagram of the satellite total zonal velocity (V_t) variability against latitude and time for the tracks S3A-385 (a) and S3A-322 (b), representing the western and eastern basins, respectively. Tracks S3A-265 and S3A-057 are not presented due to the narrowness of the shelf at these locations. The use of time-latitude HM diagrams enables qualitatively identifying the alternance among periods dominated by either eastward or westward circulation, in addition, to providing the latitudinal variability of the main flows. Even though the different tracks are not contemporary, it is possible to appreciate a generic and common winter-summer seasonality.

For track S3A-385 (Fig. 8a), the HM diagram shows some intense westward events extending along the entire transect (E1, E4 and E5). Those events can also be identified in Fig. 6 and seem to be the result of the joint action of both V_w and V_{gd} west-bounded components. These events are not limited to the shelf section but extend further offshore, potentially due to the action of Levantes along the whole basin. Additional westward events can be found more limited to the northern section and the shelf (i.e., E2 and E3), agreeing with the expected configuration of intense CCC events. As can be observed in Figure 6, E2 and E3 are mainly explained by the V_{gd} flow, suggesting that westward flows due to geostrophic forces might result in narrower coastal flows than those where also the V_w contribute. Considering that the wind-driven flows would be due to a homogeneous wind field blowing toward the west all over the GoC, they can be expected to cover an extension as wide as the mentioned wind field. On the other hand, the extension of westward flows caused only or mainly by geostrophic forces could result in narrower extensions due to constraints such as bathymetry. The southern half of the HM diagram in Fig. 8a presents the highest positive flow velocities mostly limited up to 36.6° N, agreeing with the spatial characteristics of the GoC Current (GCC). Results from track S3A-322 (Fig. 8b) show remarkably high-intensity negative flows over the southern section of the analysed transect, which most of the time extend up to the northern limits. As previously mentioned, (De Oliveira Júnior et al., 2022) performed a similar analysis based on HFR data over the GoC, and, for the eastern basin found that negative flows tend to occur mostly over the outer shelf, in line with these results that show how the most intense negative flows tend to occur more detached from the coast. Such setup of the circulation might be explained by the proximity to the Strait of Gibral-

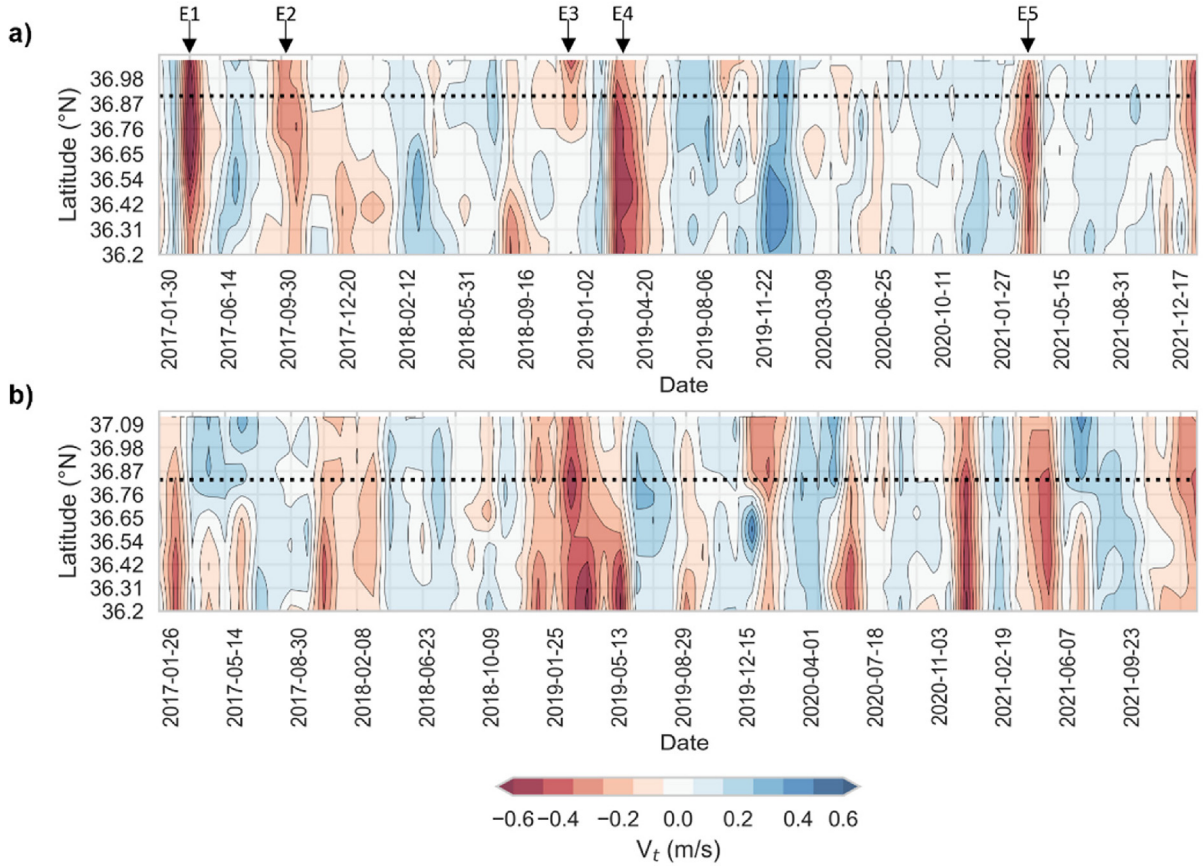

Fig. 8. Latitude-time Hovmöller diagrams of the total surface zonal velocity for the period 2017–2021 from tracks S3A-385 (a) and S3A-322 (b) Horizontal dotted lines indicate the latitude corresponding to the 200 m depth isobath.

Table 3
Monthly percentage of occurrence of westward and eastward circulation and zonal wind over the continental shelf of the GoC from Sentinel-3A tracks #385, #365, #057, #322 and NCEP-GFS wind model. Periods coloured in blue represent the dominance of eastward circulation, while those coloured in red stand for the dominance of westward circulation.

S3A Tracks	V_t Direction	Jan	Feb	Mar	Apr	May	Jun	Jul	Aug	Sep	Oct	Nov	Dec
#385	Westward	42.86	50.00	40.00	80.00	42.86	20.00	0.00	16.67	57.14	60.00	33.33	42.86
	Eastward	57.14	50.00	60.00	20.00	57.14	80.00	100.00	83.33	42.86	40.00	66.67	57.14
#365	Westward	66.67	60.00	42.86	60.00	20.00	16.67	28.57	40.00	40.00	50.00	83.33	66.67
	Eastward	33.33	40.00	57.14	40.00	80.00	83.33	71.43	60.00	60.00	50.00	16.67	33.33
#057	Westward	66.67	100.00	66.67	40.00	40.00	33.33	33.33	40.00	60.00	50.00	100.00	66.67
	Eastward	33.33	0.00	33.33	60.00	60.00	66.67	66.67	60.00	40.00	50.00	0.00	33.33
#322	Westward	75.00	100.00	60.00	33.33	40.00	0.00	16.67	28.57	20.00	60.00	60.00	83.33
	Eastward	25.00	0.00	40.00	66.67	60.00	100.00	83.33	71.43	80.00	40.00	40.00	16.67
Zonal Wind	**Direction**	**Jan**	**Feb**	**Mar**	**Apr**	**May**	**Jun**	**Jul**	**Aug**	**Sep**	**Oct**	**Nov**	**Dec**
	Westward	47.52	52.66	45.97	40.67	37.16	18.33	15.16	24.68	41.00	50.81	43.67	50.97
	Eastward	52.48	47.34	54.03	59.33	62.84	81.67	84.84	75.32	59.00	49.19	56.33	49.03

tar where easterly winds are canalised into the GoC and would drive the surface circulation since, as previously stated, is mainly controlled by the wind component over the eastern basin.

The percentage of occurrence of positive and negative flows over the different months, as estimated from the different tracks for the shelf section are presented in Table 3. This table provides a global perspective of the temporal and seasonal variability of the dominant flow direction along the year. For all four tracks, eastward circulation prevails during May, June, July and August. The prevalence of eastward flows during the spring-summer months agrees with the upwelling season, though such seasonality over the GoC is not clearly defined, during these months westerly winds are most likely to drive the surface circulation over the area (Garel et al., 2016; De Oliveira Júnior et al., 2022; Sánchez and Relvas, 2003). The opposite situation is observed for winter months, from December to February, when the cir-

culation is predominantly westward. More prevailing westward flows during winter months are associated with strong easterly winds and the effect of the along-shore sea level gradient during relaxed upwelling conditions. The resulting all-year percentages for all tracks are mainly balanced, agreeing with the results presented in (Teles-Machado et al., 2007), and with the latest study over the area (Sirviente et al., 2023) which, based on HFR measurements and numerical model simulations, found that for summer months westward flows are of smaller amplitude, and greater amplitudes are observed in eastward flows. It is worth noting that the values presented in Table 3 are based on satellite passes with 27-day cycles, resulting in approximately 5 passes per track and month for the whole period analysed.

5. Summary and conclusions

This study presents a generic methodology for assessing the surface circulation over the northern shelf of the Gulf of Cádiz, based on satellite altimetry measurements and considering the effects of ageostrophic factors such as the bottom-drag and wind-driven circulation. The results from the applied methodology were validated against in-situ measurements over the GoC's shelf. After ensuring the good performance of the methods, the outputs were applied for a characterisation of the surface circulation over the GoC northern shelf, specifically, based on 4 years of high-resolution satellite altimetry data from Sentinel-3A and wind model data. The resulting spatiotemporal characteristics agree with the general description of the literature, furthermore, the results bring additional details about the sea level variability along the GoC.

The use of the ADT construction employing MDT, for computing surface geostrophic velocities, yielded the best correlation (0.77) and the lowest root mean square error (0.10 m/s) when compared to ADCP measurements from near-shore moorings. While geoid-based methods also provided reasonable results, they exhibited slightly lower correlation coefficients and larger RMSE values. This analysis is consistent with results from prior studies in other coastal regions, such as coastal areas over the Northwest Atlantic Shelf (Feng et al., 2023), emphasizing the importance of constructing ADT based on MDT for improved accuracy, particularly in areas near the coast. Thus, the present work provides valuable insights into the choice of ADT construction methods for enhancing the reliability of satellite-derived ocean current velocity data in coastal regions.

The comparison of surface bottom-drag corrected geostrophic (V_{gd}) and total (V_t) zonal current velocity estimates derived from different altimetry-based sources, including high-resolution along-track Sentinel-3A data (S3-V_{gd} and S3-V_t) and Copernicus Marine Environment Monitoring Service (CMEMS) products (C-V_{gd} and C-V_t), with in-situ ADCP measurements, revealed that the CMEMS's geostrophic current product (C-V_{gd}) had the poorest performance due to its limited resolution. However, when incorporating wind-driven current estimates (C-V_t), the product improved significantly, emphasizing the importance of wind on the surface circulation (Mulero-Martínez et al., 2021). The best results were achieved with high-resolution altimetry data (S3A-V_{gd} and S3A-V_t). S3A-V_{gd} showed a high correlation even without wind data, with a slight bias. S3-V_t, which included wind-driven current variability, outperformed all other products in terms of statistical metrics, accurately capturing surface circulation direction most of the time. These findings encourage the use of high-resolution altimetry data as inputs for global products/models, even over coastal areas. In addition, they highlight the necessity of properly characterising local effects as wind-driven currents to reach a good understanding of the circulation over complex coastal areas.

The analysis of the surface circulation along the continental shelf aimed to assess the contributions of the bottom-friction corrected geostrophic (V_{gd}) and wind-driven (V_w) flow components to the total surface current (V_t). The results showed distinct characteristics over the different parts of the GoC. Tracks S3A-385 and 265, located in the western basin, suggested that positive (eastward) surface currents were predominantly driven by westerly winds, while only occasionally, westward flows coincided with easterly winds. These patterns suggest a higher control of the geostrophic component over westward flows, which are mainly driven by cross-shore and alongshore sea level gradients. In contrast, track S3A-322, located in the eastern basin, displayed a stronger correspondence between both V_{gd} and V_w with V_t. This fact suggests that both eastward and westward flows along the shelf in this region were primarily driven by favourable winds. These winds also induced cross-shelf sea level gradients through Ekman transport, enhancing the westward geostrophic component of the flow. Related to that, the analysis of ADT values along the whole basin showed the presence of ADT gradients, both along-shore and cross-shore, along the GoC's shelf, with a greater amplitude attributed to alongshore gradients. Notably, average alongshore ADT differences reached up to 4 cm between the easternmost and westernmost tracks. This discrepancy in ADT along the basin supports the fact that an imbalance in the along-shore pressure gradient would induce a westward flow during periods of weakened westerly winds and intensify under easterly wind conditions. These findings are consistent with the observed contributions of different components to the total shelf circulation over the different basins. They also corroborate previous studies suggesting that an alongshore pressure gradient is a primary driver of the coastal CCC under weak wind conditions (De Oliveira Júnior et al., 2021,2022) and with the observations from (Sirviente et al., 2023) of sea surface height across-shore gradients directed seawards for days when the CCC in the GoC is present.

Regarding the spatiotemporal characterisation of the surface circulation, the results for the continental shelf of the western basin showed the occurrence of westward flows primarily in the northern half of the transect, aligning with the

expected configuration of CCC events in this area. The southern half of the transect exhibited a higher occurrence of positive (eastward) flows, typically limited to latitudes up to 36.6°N, consistent with the Gulf of Cadiz Current (GCC). These findings supported previous research that found negative flows extending toward the shelf break 60–70 % of the time, with positive flows dominating further offshore. In contrast, results for the eastern basin displayed notably high-intensity negative flows, primarily in the southern section of the transect. These observations were in line with previous studies indicating that negative flows tend to occur mostly over the outer shelf and detached from the coast at the eastern basin (De Oliveira Júnior et al., 2022), as easterly winds channelled into the Gulf of Cadiz played a significant role in driving surface circulation. Across all four tracks, the eastward circulation dominated during the spring and summer months (May, June, July, and August). This eastward flow pattern correlated with the upwelling season in the Gulf of Cadiz, driven by westerly winds. In contrast, westward flows prevailed during the winter months (December to February). This westward flow predominance in winter might be associated with a higher occurrence of easterly winds and the rebalancing of the along-shore sea level gradient during relaxed upwelling conditions.

These results represent an advance in the use of satellite altimetry data for oceanographic applications in coastal areas where both the spatial and temporal variability of the circulation are highly complex. Furthermore, considering the similarity of the results with previous studies based on in-situ systems that entail more costs for the user, such as HFR and ADCP, the use of altimetry data and publicly accessible wind models is an advantage for the evaluation of oceanographic characteristics in areas with difficult access or few resources, which can contribute to a better understanding and management of coastal areas.

CRediT authorship contribution statement

R.Mulero-Martinez: Conceptualization, Data curation, Writing – original draft, Visualization, Investigation, Validation, Formal analysis, Methodology, Resources, Project administration and Software. **J.Gómez-Enri:** Conceptualization, Writing – review & editing, Investigation, Validation, Methodology, Supervision, Resources. **L.De Oliveira Júnior:** Conceptualization, Writing – review & editing, Investigation, Validation, Methodology. **E.Garel:** Conceptualization, Writing – review & editing, Investigation, Validation, Methodology. **P.Relvas:** Writing – review & editing, Investigation. **R.Mañanes:** Conceptualization, Writing – review & editing, Investigation, Validation, Methodology.

Declaration of competing interest

The authors declare that they have no known competing financial interests or personal relationships that could have appeared to influence the work reported in this paper.

References

Aldarias, A., Gomez-Enri, J., Laiz, I., Tejedor, B., Vignudelli, S., Cipollini, P., 2020. Validation of Sentinel-3A SRAL coastal sea level data at high posting rate: 80 Hz. IEEE Trans. Geosci. Remote Sens. 58 (6), 3809–3821. https://doi.org/10.1109/TGRS.2019.2957649.

Bouffard, J., Pascual, A., Ruiz, S., Faugère, Y., Tintoré, J., 2010. Coastal and mesoscale dynamics characterization using altimetry and gliders: a case study in the Balearic Sea. J. Geophys. Res. Oceans 115 (10). https://doi.org/10.1029/2009JC006087.

Bowden, K.F., 1983. Physical Oceanography of Coastal Waters. Camelot Press Ltd..

Carvalho, D., Rocha, A., Gómez-Gesteira, M., Silva Santos, C., 2014. Offshore wind energy resource simulation forced by different reanalyses: comparison with observed data in the Iberian Peninsula. Appl. Energy 134, 57–64. https://doi.org/10.1016/j.apenergy.2014.08.018.

Cleveland, W.S., Devlin, S.J., 1988. Locally weighted regression: an approach to regression analysis by local fitting. J. Am. Stat. Assoc. 83 (403), 596–610. https://doi.org/10.1080/01621459.1988.10478639.

Criado-Aldeanueva, F., García-Lafuente, J., Vargas, J.M., Jorge Del Río, A., Vázquez, A.R., Sánchez, A., 2006. Distribution and circulation of water masses in the Gulf of Cadiz from in situ observations. Deep-Sea Res. Part II: Topical Stud. Oceanogr. 53 (11–13), 1144–1160. https://doi.org/10.1016/j.dsr2.2006.04.012.

Criado-Aldeanueva, F., Garcia-Lafuente, J., Navarro, G., Ruiz, J., 2009. Seasonal and interannual variability of the surface circulation in the eastern Gulf of Cadiz (SW Iberia). J. Geophys. Res. Oceans 114 (1). https://doi.org/10.1029/2008JC005069.

De Oliveira Júnior, L., Garel, E., Relvas, P., 2021. The structure of incipient coastal counter currents in South Portugal as indicator of their forcing agents. J. Marine Syst. 214 (October 2020). https://doi.org/10.1016/j.jmarsys.2020.103486 103486.

Dinardo, S., Fenoglio-Marc, L., Becker, M., Remko Scharroo, M., Fernandes, J., Staneva, J., Grayek, S., Benveniste, J., 2021. A RIP-based SAR Retracker and its application in north East Atlantic with Sentinel-3. Adv. Space Res. 68 (2), 892–929. https://doi.org/10.1016/j.asr.2020.06.004.

Feng, H., Egido, A., Vandemark, D., Wilkin, J., 2023. Exploring the potential of Sentinel-3 delay doppler altimetry for enhanced detection of coastal currents along the Northwest Atlantic shelf. Adv. Space Res. 71 (1), 997–1016. https://doi.org/10.1016/j.asr.2022.09.011.

Fenoglio-Marc, L., Dinardo, S., Scharroo, R., Roland, A., Dutour Sikiric, M., Lucas, B., Becker, M., Benveniste, J., Weiss, R., 2015. The german bight: a validation of CryoSat-2 altimeter data in SAR mode. Adv. Space Res. 55 (11), 2641–2656. https://doi.org/10.1016/J.ASR.2015.02.014.

Folkard, A.M., Davies, P.A., Fiúza, A.F.G., Ambar, I., 1997. Remotely Sensed Sea Surface thermal patterns in the Gulf of-Cadiz and the strait of Gibraltar: variability, correlations, and relationships with the Surface wind field. J. Geophys. Res. C: Oceans 102 (C3), 5669–5683.

Förste, C.h., Bruinsma, S.L., Abrikosov, O., Lemoine, J.M., Schaller, T., Götze, H.J., Ebbing, J., Marty, J.C., Flechtner, F., Balmino, G., Biancale, R., 2014. The latest combined global gravity field model including GOCE Data up to degree and order 2190 of GFZ potsdam and GRGS toulouse. Population (Paris) 11, 25–28.

Fu, L.L., Chelton, D.B., Traon, P.Y.L., Morrow, R., 2010. Eddy dynamics from satellite altimetry. Oceanography 23 (4), 15–25. https://doi.org/10.5670/OCEANOG.2010.02.

García-Lafuente, J., Delgado, J., Criado-Aldeanueva, F., Bruno, M., del Río, J., Vargas, J.M., 2006. Water mass circulation on the continental shelf of the Gulf of Cádiz. Deep-Sea Res. Part II: Topical Stud. Oceanogr. 53 (11–13), 1182–1197. https://doi.org/10.1016/j.dsr2.2006.04.011.

Garel, E., Laiz, I., Drago, T., Relvas, P., 2016. Characterisation of coastal counter-currents on the inner shelf of the Gulf of Cadiz. J. Mar. Syst. 155, 19–34. https://doi.org/10.1016/j.jmarsys.2015.11.001.

Gómez-Enri, J., Vignudelli, S., Cipollini, P., Coca, J., González, C.J., 2018. Validation of CryoSat-2 SIRAL Sea level data in the eastern

continental shelf of the Gulf of Cadiz (Spain). Adv. Space Res. 62 (6), 1405–1420. https://doi.org/10.1016/j.asr.2017.10.042.

Gómez-Enri, J., González, C.J., Passaro, M., Vignudelli, S., Álvarez, O., Cipollini, P., Mañanes, R., Bruno, M., López-Carmona, M.P., Izquierdo, A., 2019. Wind-Induced cross-strait sea level variability in the strait of Gibraltar from coastal altimetry and in-situ measurements. Remote Sens. Environ. 221 (October 2018), 596–608. https://doi.org/10.1016/j.rse.2018.11.042.

Júnior, D.O., Luciano, P.R., Garel, E., 2022. Kinematics of Surface currents at the northern Margin of the Gulf of Cádiz. Ocean Sci. 18 (4), 1183–1202. https://doi.org/10.5194/os-18-1183-2022.

Knudsen, P., Andersen, O., Maximenko, N., 2016. The updated geodetic mean dynamic topography model - DTU15MDT. EGUGA 18 EPSC2016-5052.

Laiz, I., Plecha, S., Teles-Machado, A., González-Ortegón, E., Sánchez-Quiles, D., Cobelo-García, A., Roque, D., Peliz, A., Sánchez-Leal, R. F., Tovar-Sánchez, A., 2019. The role of the Gulf of Cadiz circulation in the redistribution of Trace metals between the Atlantic Ocean and the Mediterranean Sea. Sci. Total Environ. https://doi.org/10.1016/j.scitotenv.2019.134964.

Manso-Narvarte, I., Caballero, A., Rubio, A., Dufau, C., Birol, F., 2018. Joint analysis of coastal altimetry and High-Frequency (HF) Radar data: observability of seasonal and Mesoscale Ocean dynamics in the Bay of Biscay. Ocean Sci. 14 (5), 1265–1281. https://doi.org/10.5194/os-14-1265-2018.

Marechal, G., Ardhuin, F., Marechal, G., Ardhuin, F., 2020. Surface currents and significant wave height gradients: matching numerical models and high-resolution altimeter wave heights in the Agulhas current region. Esoar 105. https://doi.org/10.1002/ESSOAR.10505343.1 essoar.10505343.

Meloni, M., Bouffard, J., Doglioli, A.M., Petrenko, A.A., Valladeau, G., 2019. Toward science-oriented validations of coastal altimetry: application to the Ligurian Sea. Remote Sens. Environ. 224 (February), 275–288. https://doi.org/10.1016/j.rse.2019.01.028.

Morrow, R., Carret, A., Birol, F., Nino, F., Valladeau, G., Boy, F., Bachelier, C., Zakardjian, B., 2017. Observability of fine-Scale Ocean dynamics in the northwestern Mediterranean Sea. Ocean Sci. 13 (1), 13–29. https://doi.org/10.5194/OS-13-13-2017.

Mulero-Martínez, R., Gómez-Enri, J., Mañanes, R., Bruno, M., 2021. Assessment of near-shore currents from CryoSat-2 satellite in the Gulf of Cádiz using HF Radar-derived current observations. Remote Sens. Environ. 256. https://doi.org/10.1016/J.RSE.2021.112310 112310.

Mulero-martinez, R., Román-cascón, C., Mañanes, R., Izquierdo, A., Bruno, M., 2022a. "The use of sentinel-3 altimetry data to assess wind speed from the weather research and forecasting (WRF) model: application over the gulf of Cadiz. Remote Sens., 1–15

Mulero-Martinez, R., Román-Cascón, C., Mañanes, R., Izquierdo, A., Bruno, M., Gómez-Enri, J., 2022b. The use of Sentinel-3 altimetry data to assess Wind Speed from the Weather Research and Forecasting (WRF) model: application over the gulf of Cadiz. Remote Sens. 14 (16), 4036. https://doi.org/10.3390/RS14164036.

Ortega, M., Sánchez, E., Gutiérrez, C., Molina, M.O., López-Franca, N., 2023. Regional winds over the Iberian Peninsula (Cierzo, Levante and Poniente) from high-resolution COSMO-REA6 reanalysis. Int. J. Climatol. 43 (2), 1016–1033. https://doi.org/10.1002/joc.7860.

Pavlis, N.K., Holmes, S.A., Kenyon, S.C., Factor, J.K., 2008. An Earth gravitational model to degree 2160: EGM2008. Geophys. Res. Abstr. 10, 2008.

Powell, B.S., Leben, R.R., 2004. An optimal filter for geostrophic mesoscale currents from along-Track satellite altimetry. J. Atmos. Oceanic Tech. 21 (10), 1633–1642. https://doi.org/10.1175/1520-0426(2004)021<1633:AOFFGM>2.0.CO;2.

Raney, R.K., 2012. CryoSat SAR-mode looks revisited. IEEE Geosci. Remote Sens. Lett. 9 (3), 393–437. https://doi.org/10.1109/LGRS.2011.2170052.

Relvas, P., Barton, E.D., 2002. Mesoscale patterns in the Cape São Vicente (Iberian Peninsula) upwelling region. J. Geophys. Res. Oceans 107 (C10), 28–121. https://doi.org/10.1029/2000JC000456.

Roesler, C.J., Emery, W.J., Kim, S.Y., 2013. Evaluating the use of high-frequency radar coastal currents to correct satellite altimetry. J. Geophys. Res. Oceans 118 (7), 3240–3259. https://doi.org/10.1002/JGRC.20220.

Sánchez, R.F., Mason, E., Relvas, P., da Silva, A.J., Peliz, Á., 2006. On the inner-shelf circulation in the northern Gulf of Cádiz, southern Portuguese shelf. Deep Sea Res. Part II 53 (11–13), 1198–1218. https://doi.org/10.1016/J.DSR2.2006.04.002.

Sánchez, R.F., Relvas, P., 2003. Spring-Summer climatological circulation in the upper layer in the region of Cape St. Vincent, Southwest Portugal. ICES J. Mar. Sci. https://doi.org/10.1016/S1054-3139(03)00137-1.

Sirviente, S., Bolado-Penagos, M., Gomiz-Pascual, J.J., Romero-Cózar, J., Vázquez, A., Bruno, M., 2023. Dynamics of atmospheric-driven surface currents on the Gulf of Cadiz continental shelf and its link with the strait of Gibraltar and the Western Alboran Sea. Prog. Oceanogr. 219. https://doi.org/10.1016/j.pocean.2023.103175.

William, C.S., Joseph, B.K., Jimy, D., David, O.G., Zhiquan, L., Judith, B., Wei, W., Jordan, G.P, Michael, G.D., Dale, M.B., Huang, X.-Y., 2019. A Description of the Advanced Research WRF Model Version 4. NCAR Technical Note NCAR/TN-475+STR 145.

Srinivasan, M., Tsontos, V., 2023. Satellite altimetry for ocean and coastal applications: a review. Remote Sens. 15 (16), 3939. https://doi.org/10.3390/RS15163939.

Teles-Machado, A., Peliz, Á., Dubert, J., Sánchez, R.F., 2007. On the onset of the Gulf of Cadiz coastal countercurrent. Geophys. Res. Lett. 34 (12), 1–5. https://doi.org/10.1029/2007GL030091.

Troupin, C., Pascual, A., Valladeau, G., Pujol, I., Lana, A., Heslop, E., Ruiz, S., Torner, M., Picot, N., Tintoré, J., 2015. Illustration of the Emerging capabilities of SARAL/AltiKa in the coastal zone using a multi-platform approach. Adv. Space Res. 55 (1), 51–59. https://doi.org/10.1016/J.ASR.2014.09.011.